



HYBRID MODIFIERS FOR Ti DENTAL IMPLANTS

Crina ANASTASESCU,^a Diana PELINESCU,^b Ionela AVRAM,^b Emilian CHIFOR,^{*c} Ion BORDEIANU,^c
Veronica BRATAN,^a Silviu PREDA,^a Catalina GIFU,^d Elvira ALEXANDRESCU,^d
Mihai ANASTASESCU,^a Maria ZAHARESCU^a and Ioan BALINT^{*a}

^aInstitute of Physical Chemistry “Ilie Murgulescu”, 202 Splaiul Independentei, 060021 Bucharest, Roumania

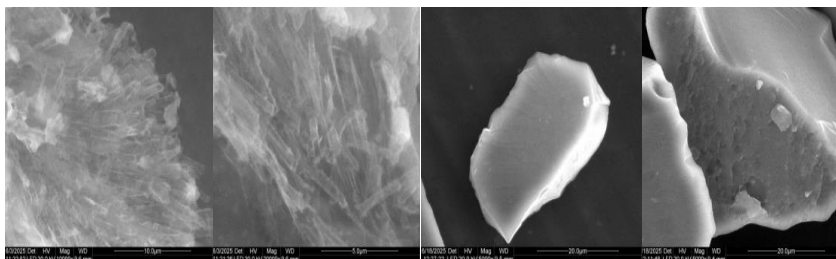
^bFaculty of Biology, Intrarea Portocalilor 1–3, Sector 5, 060101 Bucharest, Roumania

^cFaculty of Medicine, Ovidius University, Aleea Universitatii nr. 1, 900470 Constanța, Roumania

^dNational Research and Development Institute for Chemistry and Petrochemistry – ICECHIM, 202 Splaiul Independentei, 060021 Bucharest, Roumania

Received September 13, 2025

The development of hybrid nanomaterials for biomedical applications has attracted significant interest over the last decade. Accordingly, various inorganic matrices and their hybrid derivatives obtained by loading them with functional organic compounds have been developed for use in biomedical technologies and healthcare. In this



study, biocompatible matrices (SiO₂, TiO₂, IrTiO₂) obtained by the sol-gel method were used herein to develop and test their hybrid derivatives with aminolevulinic acid and Protoporphyrin IX (known photosensitizer in biological systems) as bioactive coatings for Ti dental implants. Herein, the ability of Protoporphyrin IX (which is produced in living cells from aminolevulinic acid) as well as that of the inorganic carriers (SiO₂ with tubular morphology, TiO₂, IrTiO₂), to photogenerate reactive oxygen species—especially singlet oxygen—when exposed to light is envisaged. The inorganic materials and their hybrid derivatives were characterised by using Scanning Electron Microscopy (SEM), X-ray Diffraction (XRD), UV-Vis Spectroscopy (UV-Vis), Photoluminescence Spectroscopy (PL), and zeta potential measurements. The cytotoxicity of oxidic matrices modified with aminolevulinic acid was evaluated using *Saccharomyces cerevisiae* 10701 as a model eukaryotic organisms. The time-dependent photogeneration of singlet oxygen in the presence of SiO₂, TiO₂, IrTiO₂ matrices modified with Protoporphyrin IX was monitored by Photoluminescence Spectroscopy using dimethylantracene as a probe under visible-light irradiation. The antibacterial activity of Protoporphyrin IX-modified SiO₂, TiO₂, and IrTiO₂ was assessed against the reference strain *Staphylococcus aureus* ATCC 29213.

INTRODUCTION

Innovative biomaterials have attracted great interest, as the healthcare field has gathered significant logistical and human resources over the

past decade. The use of inorganic matrices as carriers for functional compounds with biological applications is a well-established approach that has been extensively explored to date. Moreover, the intrinsic bioactivity of certain inorganic structures—

* Corresponding authors: ibalint@icf.ro (I.B.); chifor.emil@yahoo.com (E.C)

particularly photoactive oxides, carbon-based derivatives)¹ offers a valuable advantage. These materials are generally capable of generating reactive oxygen species (hydroxyl radicals $\bullet\text{OH}$, hydrogen peroxide H_2O_2 , superoxide anions $\bullet\text{O}_2^-$, and singlet oxygen $^1\text{O}_2$) upon illumination which enable them to act effectively against pathogens, including bacterial biofilms and viruses.^{2,3} Among the reactive oxygen species, singlet oxygen – a nonradical form-, exhibits significant activity not only in biological systems⁴ but also in environmental remediation processes, fine chemical synthesis, light-assisted therapies such as photodynamic therapy⁵ (PDT), and blood sterilization. Photodynamic therapy, which relies on the antitumor activity of singlet oxygen, is a procedure that is widely studied and increasingly used today due to its low adverse effects and minimal invasiveness. This process requires the presence of a sensitizer, molecular oxygen (O_2), and a photoactive material capable of generating singlet oxygen under light irradiation at specific, appropriate wavelengths.⁶ The efficiency of this mechanism can be enhanced through various strategies, including the modulation of tumor hypoxia.⁷ According to De Rosa *et al.*,⁸ the most commonly employed singlet oxygen generators are organic compounds such as porphyrins, phthalocyanines as well as inorganic materials including transition metal complexes of ruthenium, platinum, palladium, in addition to photoactive oxides. The same authors emphasize some advantages associated with supporting organic photosensitizers on solid carriers, including their reusability and ease of recovery in water purification processes which positively influence on overall economic feasibility. Additionally, immobilization facilitates the separation of the photosensitizer from reaction products in photochemical syntheses. Generally, the main drawback of singlet oxygen generation using immobilized photosensitizers, compared with free ones, is the lower quantum yield; however, in the present study, this limitation can be modulated by the intrinsic contribution of the carrier material.

Protoporphyrin IX is naturally present in humans and living cells as a precursor of heme, while also exhibiting distinct biological functions. However, its excessive accumulation can induce skin photosensitivity and damage to the liver.⁹ Due to its ability to generate singlet oxygen, PpIX has been used in cancer therapy through photodynamic mechanisms¹⁰. The indirect application of PpIX in

photodynamic therapy (PDT) arises from its endogenous biosynthesis in tissues from aminolevulinic acid.^{10,11} 5-Aminolevulinic acid (ALA) is involved in the biosynthesis of tetrapyrroles found in porphyrins, heme and vitamin B12.¹¹ Aminolevulinic acid has various applications in: a) agriculture (as a biodegradable herbicide and insecticide, and as a growth-promoting factor; b) medicine (for the diagnosis of heavy-metal poisoning and porphyria, and in cancer treatment); c) biotechnology (for the production of heme-containing enzyme, porphyrin, Vitamin B12).¹¹ Metallic nanoparticles (Au)^{12,13} have been used as a carrier for aminolevulinic acid-based photodynamic cancer therapy, achieving better results than free aminolevulinic acid.

Our previous work explored the use of nanoparticles (NPs) – both metallic (Au , Ag NPs) and semiconductor oxides (TiO_2) – to improve the Ti dental implants.¹⁴ These studies focused on singlet oxygen ($^1\text{O}_2$) generation by inorganic coatings exposed to visible light irradiation as well as on their antibacterial behavior before and after modification with metallic nanoparticles (Au , Ag) and lysozyme. Another inorganic material-an insulator with atypical optically active properties developed in successive studies¹⁵ – namely tubular SiO_2 , both bare and embedded in PVA, was modified with Au nanoparticles and Ruthenizer dye and investigated for its ability to generate singlet oxygen under visible light irradiation. The antibacterial activity was tested against *S. aureus*¹⁶ under irradiation with visible light. Furthermore, tubular SiO_2 was loaded with Ir and IrO_x nanoparticles as well as porphyrins, in order to enhance singlet oxygen photogeneration, whose reactivity was evaluated using α tocopherol¹⁷ as a target molecule.

Based on these previous results, the present work advances a practical approach for using these materials as follows: the development of hybrid coatings for dental Ti implants endowed with antibacterial activity through the photogeneration of ROS, particularly singlet oxygen, under visible-light irradiation, while also exploring their potential application in photodynamic therapy. Accordingly, this study aims to synthesize and characterize, using physicochemical methods, samples of SiO_2 , TiO_2 and IrTiO_2 modified with 5-Aminolevulinic acid and Protoporphyrin IX (SiO_2LA , TiO_2LA , IrTiO_2LA ; SiO_2P , TiO_2P , IrTiO_2P). In addition, their functional properties are evaluated as follows: a) the cytotoxicity of

aminolevulinic acid-modified oxides was tested on *Saccharomyces cerevisiae*; b) the capacity of SiO_2 , TiO_2 , IrTiO_2 matrices modified with Protoporphyrin IX to generate singlet oxygen under visible-light irradiation was monitored using dimethylanthracene; c) the antibacterial activity of the Protoporphyrin IX-modified samples against *S.aureus* after irradiation with visible-light irradiation was assessed. The novelty of the results stems from the combined functionality exhibited by these hybrid materials, arising from both the photosensitizer and the intrinsic, atypical activity of the inorganic matrices. In this study, protoporphyrin IX is valorized through two distinct approaches: directly, by developing its hybrids with the selected inorganic matrices, and indirectly, by using aminolevulinic acid as precursor. Future extended studies are planned to develop and characterize biosynthesized protoporphyrin IX obtained from aminolevulinic acid and incorporated

into inorganic matrices. The systems proposed herein may represent an alternative in clinical practice to already approved and commercially available products (e.g, "Aladent"), which contain aminolevulinic acid as precursor of protoporphyrin IX.

RESULTS AND DISCUSSION

1. SEM

Figure 1 presents SEM images of the investigated inorganic materials. Figs. 1a, b show transparent, thin tubes with diameters of several hundred nanometers, rectangular shapes, and open ends. Figure 1c presents monolithic aggregates of TiO_2 nanoparticles that retain their compact structure after the addition of iridium nanoparticles, which cannot be distinguished in the SEM images.

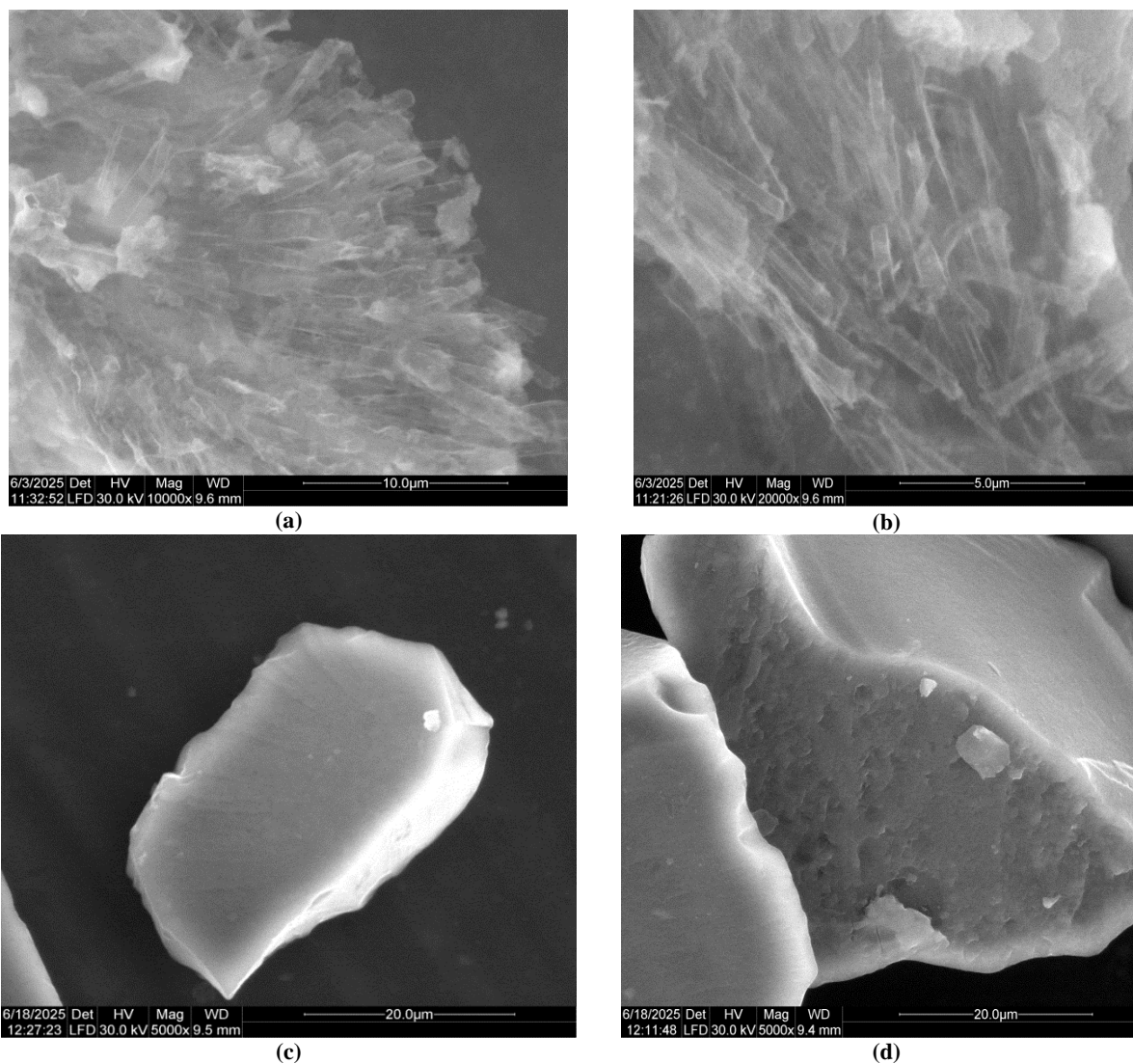


Fig. 1 – SEM images of SiO_2 (a,b); TiO_2 (c) and IrTiO_2 (d) powders.

2. XRD

Figure 2 indicates an amorphous structure for SiO₂ nanotubes, consistent with previous reports.^{15–17} The figure also shows the presence of anatase as the

crystalline phase of TiO₂ and, in the case of the IrTiO₂ sample, metallic iridium nanoparticles in addition to anatase. The crystallite size was determined to be 24 nm for iridium and 8 nm for anatase.

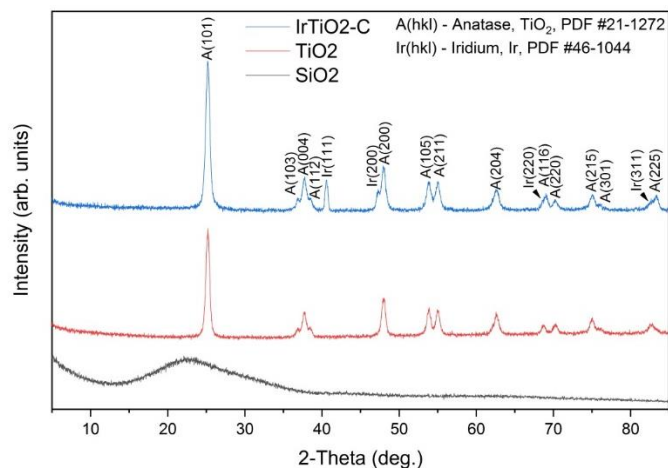


Fig. 2 – XRD pattern of the inorganic samples.

3. UV-Vis

Figure 3 presents the UV–Vis spectra of hybrids based on SiO₂, TiO₂ and IrTiO₂.

Consistent with previous works,^{15–17} tubular SiO₂ shows a high capacity for light harvesting, largely due to the enrichment achieved through optimized synthesis.

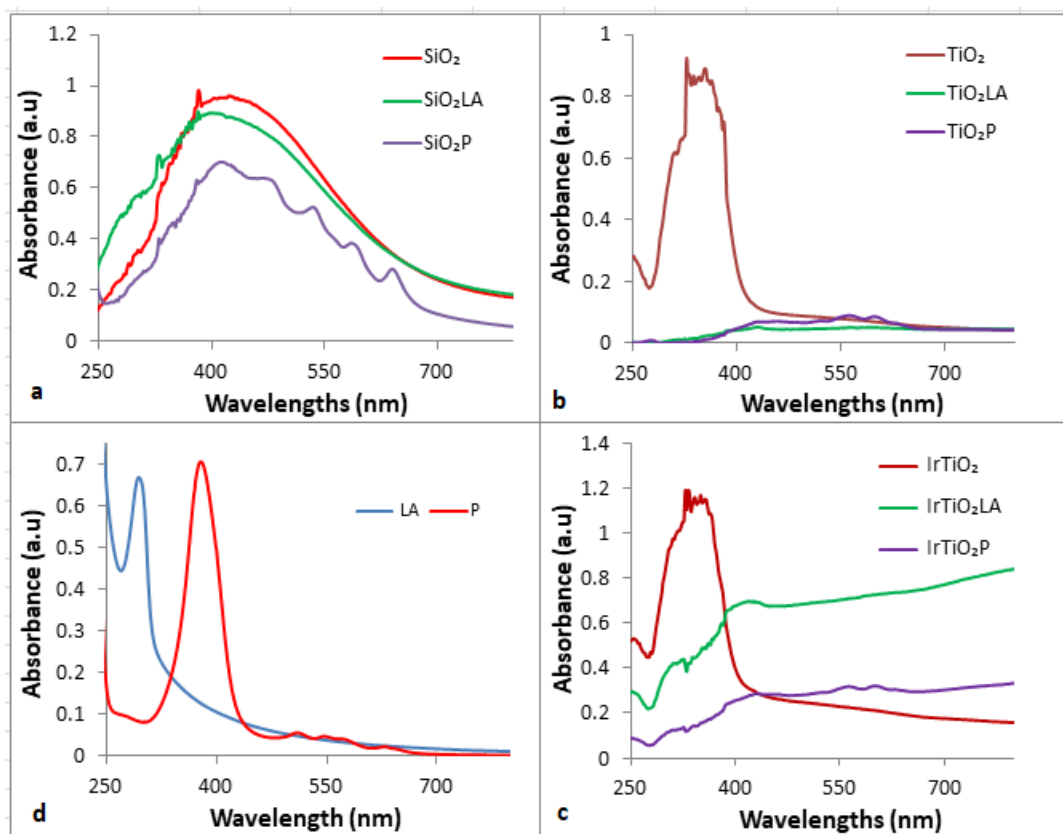


Fig. 3 – UV-Vis spectra of the bare and modified powders with aminolevulinic acid and protoporphyrin IX: a) SiO₂; b) TiO₂; c) IrTiO₂ together with the spectra of free aminolevulinic acid; d) protoporphyrin IX in liquid phase.

The addition of protoporphyrin allows for preserving the shape of the bare SiO₂ absorption curve with a small decrease in intensity. According to literature data, the “fingerprint” of Protoporphyrin IX consists of the Soret band near 400 nm and the four Q bands between 500 and 620 nm.¹⁸ These features can be observed in the absorption spectrum of the free porphyrin (P) shown in Fig. 1d as well as in Fig. 1a for the SiO₂P sample. The absorption spectra of free aminolevulinic acid are presented in Fig. 3d (LA), displaying a maximum around 300 nm which also appears as a shoulder in the absorption spectrum of SiO₂ modified with aminolevulinic acid (SiO₂ LA).

In the case of TiO₂, the addition of aminolevulinic acid or protoporphyrin IX leads to a sharp decrease in light absorption (Fig. 1b). A slight presence of porphyrin can be identified in the 500–650 nm range.

For the IrTiO₂LA and IrTiO₂P samples, the same significant decrease in UV range absorption is observed relative to unmodified IrTiO₂, however, an increase in absorbance is evident in the visible region. This difference is due to the presence of Ir nanoparticles, which enhance light absorption compared with the TiO₂ sample (Fig. 3b).

4. Fluorescence

Photoluminescence measurements reveal emission bands for SiO₂, TiO₂ and IrTiO₂ centered at 631 and 700 nm, showing a slight red shift compared with the results reported by Rossi *et al.*¹⁸ for protoporphyrin IX loaded on spherical silica. The PL signal is significantly higher for the SiO₂ carrier than for TiO₂ and IrTiO₂ indicating a more efficient loading of SiO₂ matrix with porphyrin.

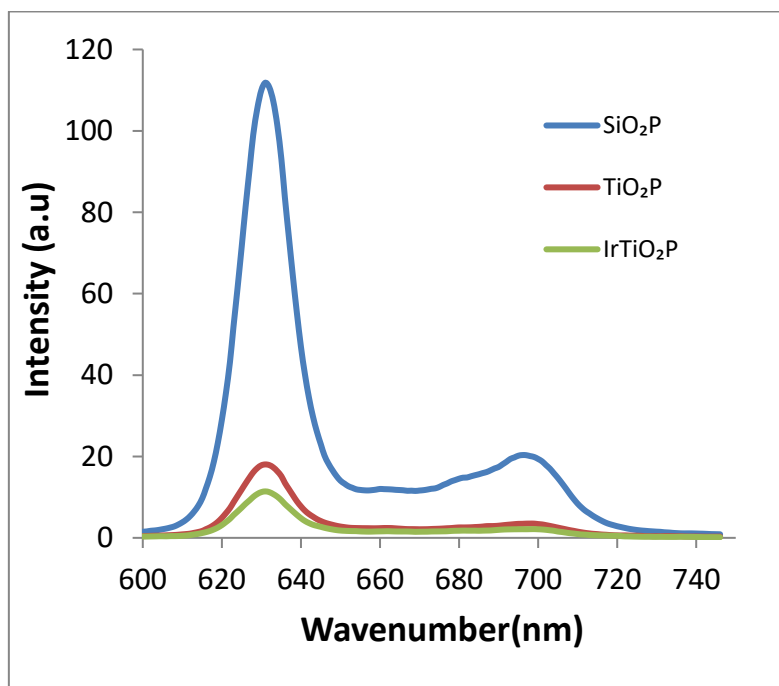


Fig. 4 – Photoluminescence signal of Protoporphyrin IX loaded onto SiO₂, TiO₂, IrTiO₂ samples for $\lambda_{\text{ex}} = 400$ nm, measured in water at room temperature.

5. Zeta Potential Measurement

Figure 5 illustrates the surface charge of the inorganic matrices before and after loading with aminolevulinic acid and protoporphyrin IX, with zeta potential measurements showing negative values in all cases. Porphyrin loading causes a more pronounced decrease in the zeta potential of bare SiO₂ compared to aminolevulinic acid ($-16 \text{ mV}_{\text{SiO}_2} \rightarrow -25.6 \text{ mV}_{\text{SiO}_2\text{P}} \rightarrow -21.7 \text{ mV}_{\text{SiO}_2\text{LA}}$). The TiO₂ surface exhibits the greatest negative charge after

porphyrin loading ($-21.6 \text{ mV}_{\text{TiO}_2} \rightarrow -30.8 \text{ mV}_{\text{TiO}_2\text{P}}$) but is slightly raised towards more positive values by the presence of aminolevulinic acid ($-21.6 \text{ mV}_{\text{TiO}_2} \rightarrow -18.6 \text{ mV}_{\text{TiO}_2\text{LA}}$). The IrTiO₂ matrix undergoes similar changes upon loading with the two organic modifiers, although more positive values were registered compared to TiO₂ due to the presence of metallic Ir. The recorded values clearly show that, for all the inorganic matrices, surface charge changes occur upon loading with modifiers (aminolevulinic acid and porphyrin).

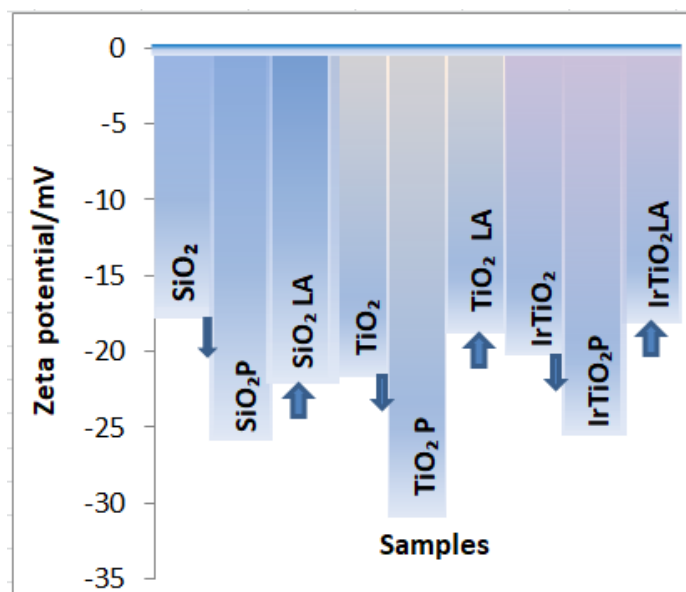


Fig. 5 – Zeta potential measurements of SiO₂, TiO₂, IrTiO₂, and their hybrids with aminolevulinic acid and protoporphyrin IX.

6. Monitoring of the singlet oxygen (¹O₂) photogeneration

The generation of singlet oxygen in the presence of SiO₂, TiO₂ and IrTiO₂-based materials is shown in Fig. 6.

Dimethylantracene is largely used for monitoring the photogeneration of singlet oxygen by fluorescence measurements^{5,19} and is known as a singlet-oxygen trapper.²⁰ Herein, using DMA with $\lambda_{\text{ex}} = 370$ nm, a decrease in fluorescence emission is

observed as singlet-oxygen production increases during 30 minutes of exposure to visible-light irradiation ($\lambda > 420$ nm). Figure 6 shows that the most pronounced decrease in the PL signal occurs for the porphyrin-modified SiO₂ matrix, with the emission bands at 426, 451 and 475 nm. Gross *et al.*²¹ monitored the oxygen-mediated photosensitization of DMA in real time by following its fluorescence decrease (recording emission bands at 408, 431 and 457 nm for $\lambda_{\text{ex}} = 360$ nm, in water).

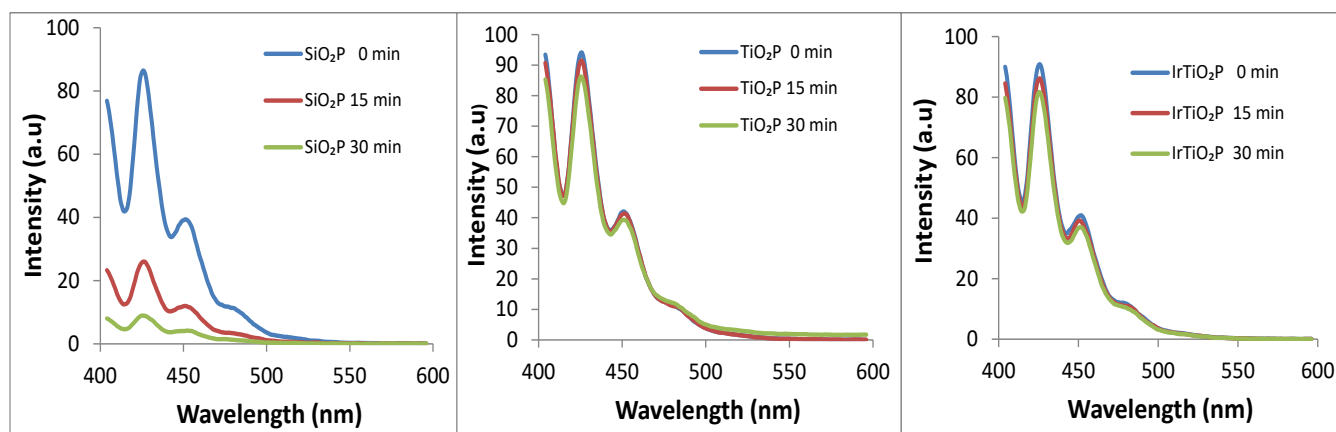


Fig. 6 – Monitoring of the singlet oxygen generation in the presence of SiO₂, TiO₂, IrTiO₂ modified with porphyrin using dimethylantracene under visible light irradiation ($\lambda > 420$ nm).

This indicates the significant ability of the porphyrin-modified SiO₂ matrix to generate singlet oxygen, reflecting the combined contribution of both components: porphyrin and optically active carrier (tubular SiO₂). For TiO₂-based hybrids, only a slight decrease in the emission bands is observed, most likely attributable to the porphyrin acting as a

singlet-oxygen generator. This decrease is more pronounced for the IrTiO₂ sample suggesting an additional contribution from the iridium nanoparticles to singlet-oxygen photogeneration, which is consistent with the literature reports on singlet oxygen-sensitized photogeneration by metallic nanoparticles.^{22,23} Furthermore, the lack of

intrinsic photoactivity of the TiO_2 matrix under visible-light irradiation is fully expected, as supported by Figs. 3b,c.

7. Cytotoxicity test for SiO_2LA , TiO_2LA , and IrTiO_2LA

The cytotoxic effect of aminolevulinic acid loaded onto the inorganic matrices was evaluated by

monitoring the growth of *S. cerevisiae* cultures. The results showed that the aminolevulinic acid alone did not significantly impair yeast growth, indicating that it is non-toxic at the tested concentration. A slight inhibitory effect was observed for the SiO_2 -based nanomaterials compared with the TiO_2 nanoparticles (Fig. 7). An increased growth relative to the negative control (C) was recorded for the TiO_2Ir nanoparticles. As expected, the positive control (fluconazole) inhibited yeast cell viability.

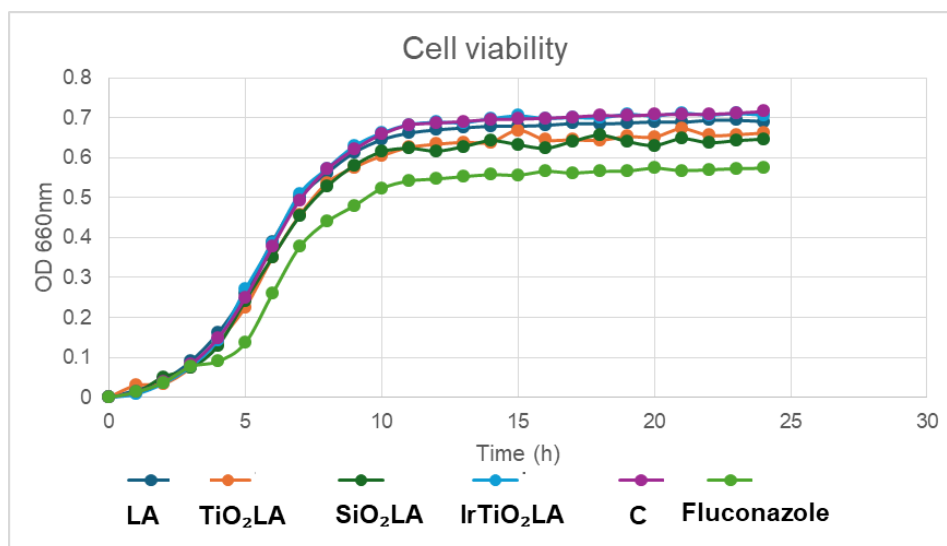


Fig. 7 – Cell viability of *S. cerevisiae* in the presence of hybrid materials (LA- aminolevulinic acid, C- untreated yeast cells).

8. Antibacterial activity against *S.aureus* under visible-light illumination

The hybrid materials investigated (SiO_2P , TiO_2P , IrTiO_2P) reduced microbial viability compared to the control (C) – Fig. 8.

The highest antimicrobial activity was observed for the porphyrin-modified SiO_2 sample (SiO_2P), which showed slightly higher activity than the free

porphyrin (P). This can be attributed to the intrinsic contribution of the SiO_2 matrix to singlet oxygen photogeneration, and the superior antimicrobial performance of the SiO_2P sample is consistent with the results shown in Fig. 6. A slight difference between TiO_2P and IrTiO_2P samples is visible in Fig. 8, with the presence of Ir nanoparticles accounting for the decrease cell viability observed for IrTiO_2P relative to the TiO_2P .

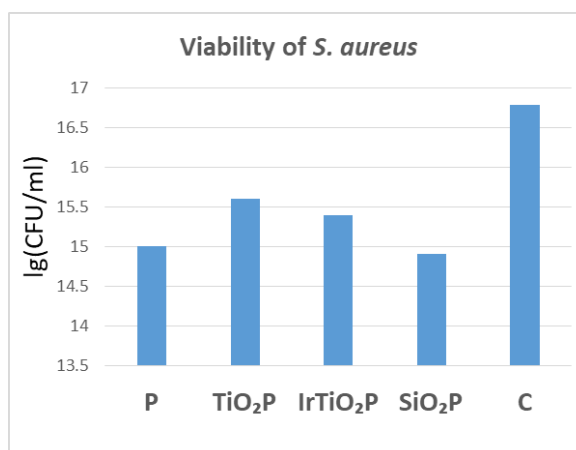


Fig. 8 – Antibacterial activity of the porphyrin-modified samples against *S. aureus* under visible-light irradiation, expressed as cell viability.

MATERIALS AND METHODS

1. Material Synthesis

1.1. SiO₂ Nanotubes

The sol–gel synthesis of SiO₂ with tubular morphology has been described in previous works.^{15–17} The precursors involved were tetraethyl orthosilicate as the silicon source (TEOS, 99%, Alfa Aesar, USA), DL tartaric acid (TA, Riedel de Haen, Germany) for the formation of ammonium tartrate, and absolute ethanol (99.5% Merck, Germany) as the solvent. The molar ratio employed was 1 TEOS/0.035 TA/21.5 C₂H₅OH/18 H₂O. Ammonia gas bubbled from a heated NH₄OH solution (30% Roth) was added to this mixture cooled to 0 °C. The obtained material was filtered, dried at 100 °C, and subjected to thermal treatment at 500 °C for 3 h. By using a) ammonium tartrate as “in situ” – formed organic template; b) fine-tuning of synthesis parameters, and c) controlled thermal treatment, SiO₂ nanotubes with optically active defects can be obtained. These defects enhance the light – harvesting capability of the resulting material.

1.2. TiO₂ nanoparticles

The synthesis of titania nanoparticles using the sol-gel method has been reported previously.^{14,24} The obtaining of titania precursor involved titanium isopropoxide (97% Aldrich), isopropyl alcohol (99.7% Lachner), 2,4-Pentadione (99% Alfa Aesar) and water. The resulting sol was allowed to age and was then thermally treated in air at 500 °C for 3 h.

1.3. IrTiO₂ nanoparticles

Iridium nanoparticles (Iridium pulv.99.9%, Fluka, Switzerland) were added to the synthesized gel (obtained as described previously) under gentle stirring. After aging, the resulting material was subjected to thermal treatment in air at 500 °C for 3 h.

1.4. Development of hybrid materials: SiO₂P, TiO₂P, IrTiO₂P and SiO₂LA, TiO₂LA, IrTiO₂LA

The pre-synthesized, thermally treated SiO₂, TiO₂ and IrTiO₂ samples were further modified as follows:

a) SiO₂P, TiO₂P, IrTiO₂P

0.005 g of Protoporphyrin IX (Protoporphyrin IX ≥ 95% Sigma Aldrich, USA) was dispersed in 6 ml mixture (1:1 vol%) of methanol (≥ 99.8%, Merck) and tetrahydrofuran (≥ 99.9%, Roth) to prepare a stock solution; Then, 0.02 g of each inorganic matrix was impregnated with 40 μl of the

porphyrin-containing stock solution, gently homogenized, and slowly dried.

b) SiO₂LA, TiO₂LA, IrTiO₂LA

0.01 g of aminolevulinic acid (5-aminolevulinic acid hydrochloride C₅H₉NO₃·HCl ≥ 98% für die Biochemie, Roth) was dispersed in 2 ml of ultrapure water (Milli-Q, >18.2 MΩ·cm) to prepare a stock solution; Then, 0.02 g of each inorganic matrix was impregnated with 40 μl of the aminolevulinic acid-containing stock solution, gently homogenized, and slowly dried.

2. Characterization Methods

2.1. SEM

The morphology of the samples was investigated by scanning electron microscopy (SEM) using an FEI Quanta 200 instrument (The Netherlands) operated at an accelerating voltage of 30 kV. Images were captured using a large field detector (LFD) in low-vacuum mode.

2.2. XRD

X-ray diffraction (XRD) patterns of the inorganic samples were obtained by using a Rigaku Ultima IV multipurpose diffraction system (Rigaku Corp., Japan) under the following conditions: 30 mA, 40 kV, and room temperature. The 2θ range was scanned from 5° to 85° with a step size of 0.02° and a scan rate 2°/min.

2.3. UV-Vis

Diffuse reflectance UV–Vis spectra of the hybrid samples were recorded using a Perkin Elmer Lambda 35 spectrophotometer. The spectra were converted to absorption spectra using the Kubelka-Munk function. For UV-Vis measurements in liquid phase (solutions containing porphyrin and aminolevulinic acid), an Analytik Jena Specord 200 Plus spectrophotometer was used.

2.4. Photoluminescence

The photoluminescence (PL) signals of the porphyrin loaded onto SiO₂, TiO₂ and IrTiO₂ matrices were measured in water, at room temperature using a Carry Eclipse fluorescence spectrometer (Agilent Technologies, USA). The operating parameters were: excitation and emission slit widths of 2.5 nm each, with a scan rate of 120 nm/min.

2.5. Zeta potential

Zeta potential measurements have been performed by using dynamic light scattering (DLS)

on a Nano Zetasizer ZS (Malvern Instruments, UK). The measurements were performed at room temperature, in triplicate.

2.6. Monitoring of Singlet Oxygen (1O_2)

Photogeneration

Singlet oxygen generation in the presence of the hybrid materials was investigated by photoluminescence (PL) spectroscopy using a Carry Eclipse fluorescence spectrometer (Agilent Technologies CA, USA), by monitoring the fluorescence decrease of 9,10-dimethylanthracene (99%, Sigma Aldrich). A quantity of 0.001 g of each hybrid material was suspended in 4 ml solution of a 1 mM DMA in acetonitrile (99.9%, Sigma Aldrich) and exposed to visible light irradiation (compact xenon light source Max 350 with a narrow band-pass filter for monochromatic irradiation $\lambda = 400$ nm, Asahi Spectra, Japan). The decrease in the PL signal of DMA was measured under the following conditions: $\lambda_{ex} = 370$ nm, excitation/emission slit widths of 2.5/2.5 nm.

2.7. Cytotoxicity

To evaluate the cytotoxic effect and potential growth inhibition, the investigated materials were tested on *Saccharomyces cerevisiae* 10701 as a model eukaryotic organisms. The yeast strain were grown in 3 ml YPG liquid medium (g/L: yeast extract 10, peptone 20, glucose 20, pH 6) in a 6 well-plate in the presence of the samples, starting from an initial concentration of 1×10^6 cells/ml. The plate was incubated at 28 °C for 24 h, and the optical density at 660 nm was measured hourly using Synergy HTX microplate spectrophotometer (BioTek Instruments, USA). As a negative control (C), *S. cerevisiae* cultures without added compounds were used, while cultures grown in the presence of fluconazole (10 μ g/ml) served as the positive control.

2.8. Bacterial Growth Inhibition Assay

The antimicrobial activity of the synthesized materials was evaluated against the reference strain *Staphylococcus aureus* ATCC 29213. Bacterial cultures were grown in Luria-Bertani (LB) broth (10 g/L peptone, 5 g/L NaCl, 5 g/L yeast extract, pH adjusted to 6.0) in the presence of the investigated materials. The initial bacterial concentration was standardized to approximately 1.4×10^6 CFU/mL. All samples were incubated at 37 °C with agitation at 150 rpm. Following incubation, bacterial viability was assessed using a serial decimal dilution assay. Aliquots (100 μ L) from appropriate dilutions were plated on solid LB agar to enable colony isolation.

Plates were incubated at 37 °C for 18–24 hours. After incubation, colonies were counted, and the number of viable bacteria was expressed as colony-forming units per milliliter (CFU/mL) calculated by multiplying the colony count by the corresponding dilution factor. The assay was performed in triplicate for each condition. As a negative control, *S. aureus* ATCC 29213 was grown in LB broth without the addition of nanoparticles.

CONCLUSIONS

Protoporphyrin IX and aminolevulinic acid were successfully loaded onto biocompatible, inorganic carriers (SiO₂ with tubular morphology, TiO₂, IrTiO₂), having in view to use the resulting hybrid materials as bioactive modifiers for Ti dental implants. Their bioactivity arises from their ability to generate singlet oxygen, a reactive oxygen species with antibacterial activity under visible light irradiation, offering potential application in photodynamic therapy.

Physicochemical investigations performed on the inorganic matrices revealed the tubular, amorphous structure of SiO₂ and anatase as the crystalline phase for TiO₂ – based samples. In addition, the light absorptive properties of these materials were demonstrated, supporting their selection for the development of hybrid materials with organic sensitizers for singlet oxygen generation.

Functional investigations of the developed hybrid materials demonstrated the significant ability of the porphyrin-modified SiO₂ sample to generate singlet oxygen under visible light irradiation which correlates with its antibacterial activity against *S. aureus*. The cytotoxicity assays on *Saccharomyces cerevisiae* indicate the potential use of aminolevulinic acid as a modifier for Ti dental implant, serving as a precursor for the biosynthesis of Protoporphyrin IX in contacted tissues and acting as a provider of singlet oxygen for the aforementioned biomedical applications.

REFERENCES

1. M.R. Younis, G. He, J. Qu, J. Lin, P. Huang, X.-H. Xia, *Adv. Sci.*, **2021**, 8, 2102587.
2. H. Xin, Y. Liu, Y. Xiao, M. Wen, L. Sheng, Z. Jia, *Adv. Funct. Mater.*, **2024**, 34, 2402607.
3. J.A. Quek, S.M. Lam, J.C. Sin, A.R. Mohamed, *J. Photochem. Photobiol. B Biol.*, **2018**, 187, 66–75.
4. I. Pibiri, S. Buscemi, A. Palumbo Piccionello, A. Pace, *ChemPhotoChem*, **2018**, 2, 535–547.

5. R. Dalapati, S. Nandi, K. Van Hecke, S. Biswas, *Cryst. Growth Des.*, **2019**, *19*, 6388–6397.
6. N. Alvarez, A. Sevilla, *Int. J. Mol. Sci.*, **2024**, *25*, 1023.
7. M. Yi, B. Xiong, Y. Li, W. Guo, Y. Huang, B. Lu, *Eur. J. Med. Chem.*, **2023**, *247*, 115084.
8. M. C. De Rosa, R. J. Crutchley, *Coord. Chem. Rev.*, **2002**, *233/234*, 351–371.
9. M. Sachar, K. E. Anderson, X. Ma, *J. Pharmacol. Exp. Ther.*, **2016**, *356*, 267–275.
10. E. R. Gallegos, I. De León Rodríguez, L. A. Martínez Guzmán, A. J. Pérez Zapata, *Archives of Med. Res.*, **1999**, *30*, 163–170.
11. K. Sasaki, M. Watanabe, T. Tanaka, T. Tanaka, *Appl. Microbiol. Biotechnol.*, **2002**, *58*, 23–29.
12. M. K. K. Oo, X. Yang, H. Du, H. Wang, *Nanomedicine*, **2008**, *3*, 777–786.
13. K. de Oliveira Gonçalves, M. Nascimento da Silva, L. Bonfante Sicchieri, F. Rodrigues de Oliveira Silva, R. Almeida de Matosa, L. Coronato Courrol, *Analyst*, **2015**, *140*, 1974–1980.
14. E. Chifor, I. Bordeianu, C. Anastasescu, J.M. Calderon-Moreno, V. Bratan, D.-I. Eftemie, M. Anastasescu, S. Preda, G. Plavan, D. Pelinescu, R. Ionescu, I. Stoica, M. Zaharescu, I. Balint, *Nanomaterials*, **2022**, *12*, 3186.
15. C. Anastasescu, C. Negrila, D. G. Angelescu, I. Atkinson, M. Anastasescu, N. Spataru, M. Zaharescu, I. Balint, *Catal. Sci. Technol.*, **2018**, *8*, 5657–5668.
16. D. Pelinescu, M. Anastasescu, V. Bratan, V.-A. Maraloiu, C. Negrila, D. Mitrea, J. Calderon-Moreno, S. Preda, I.C. Gifu, A. Stan, *Gels*, **2023**, *9*, 650.
17. M. Anastasescu, R. Socoteanu, V. Bratan, S. Preda, C. Anastasescu, I. C. Gifu, C. L. Nistor, R. Boscencu, E. Chifor, C. Negrila, I. Bordeianu, M. Zaharescu, I. Balint, *Micromachines*, **2025**, *16*, 784.
18. L. M. Rossi, P. R. Silva, L. L. R. Vono, A. U. Fernandes, D. B. Tada, M. S. Baptista, *Langmuir*, **2008**, *24*, 12534–12538.
19. A. Beltrán, M. Mikhailov, M. N. Sokolov, V. Pérez-Laguna, A. Rezusta, M. Jose Revillod, F. Galindo, *J. Mater. Chem. B*, **2016**, *4*, 5975–5979.
20. L. Gou, B. Opheim, C.N. Coretsopoulos, A.B. Scranton, *Chem. Eng. Comm.*, **2006**, *193*, 620–627.
21. E. Gross, B. Ehrenberg, F. M. Johnso, *J. Photochem. Photobiol.*, **1993**, *51*, 808–813.
22. N. Macia, R. Bresoli-Obach, S. Nonell, B. Heyne, *J. Am. Chem. Soc.*, **2019**, *141*, 684–692.
23. R. Vankayala, A. Sagadevan, P. Vijayaraghavan, C.-L. Kuo, K. C. Hwang, *Angew. Chem. Int. Ed.*, **2011**, *50*, 10640–10644.
24. C. Anastasescu, N. Spataru, D. Culita, I. Atkinson, T. Spataru, V. Bratan, C. Munteanu, M. Anastasescu, C. Negrila, I. Balint, *Chem. Eng. J.*, **2015**, *281*, 303–311.